IEEE Access
Multidisciplinary | Rapid Review | Open Access Journal

Received August 15, 2019, accepted August 31, 2019, date of publication September 5, 2019, date of current version September 23, 2019.

Digital Object Identifier 10.1109/ACCESS.2019.2939674

Generalized Least Squares Based Channel Estimation for FBMC-OQAM

VIBHUTESH KUMAR SINGH, (Student Member, IEEE), MARK F. FLANAGAN, (Senior Member, IEEE), AND BARRY CARDIFF, (Senior Member, IEEE)

School of Electrical and Electronic Engineering, University College Dublin, Dublin, D04V1W8 Ireland

Corresponding author: Vibhutesh Kumar Singh (vibhutesh.k.singh@ieee.org)

This publication has emanated from research supported by a research grant from Science Foundation Ireland (SFI) and is co-funded under the European Regional Development Fund under Grant Number 13/RC/2077.

ABSTRACT The presence of intrinsic inter-carrier interference (ICI) and inter-symbol interference (ISI) at the output of the matched filter receiver in filter bank multi-carrier with offset quadrature amplitude modulation (FBMC-OQAM) systems complicates the task of channel estimation (CE). The conventional approach is to use a pilot symbol preamble structure, such as in the interference approximation/cancellation methods (IAM/ICM), together with a simple virtual symbol (VS) based CE scheme. However, this virtual symbol approach ignores the residual interference from the data portion of the FMBC burst as well as the correlation of the noise across the sub-carriers; both of these factors ultimately limit the performance. In this paper, we propose a generalized least squares (GLS) based CE scheme which, when applied to the IAM/ICM pilot structures, takes into account both the correlated noise and data interference effects. Closed-form expressions are derived for the channel estimation mean-squared error (CE-MSE) of the proposed GLS method and for the conventional VS method, and it is shown that the proposed method leads to a significant reduction of the CE-MSE by up to 6 dB when compared with the VS based method. This is demonstrated to result in improved bit error rate (BER) performance, especially when higher-order modulation is employed, making it an attractive channel estimation method for many modern deployment scenarios. The proposed GLS-based channel estimation scheme is parameterized allowing a flexible trade-off between channel frequency selectivity, estimation complexity and CE-MSE gain. Finally, symmetry properties of the intrinsic interference coefficients for a general FBMC-OQAM system are also proved, which facilitate the computation of the noise and interference autocorrelation matrices required by the proposed algorithm.

INDEX TERMS Filter bank multi-carrier, channel estimation, generalized least squares, preamble, virtual symbol, modulation.

I. INTRODUCTION

The use of cyclic-prefixed orthogonal frequency division multiplexing (CP-OFDM) enables low-complexity equalization of wideband channels [1] and has resulted in widespread adoption in many modern communication protocols, e.g. 4G, Wi-Fi, DVB [2]. However, there are undesirable aspects of CP-OFDM which make it less favorable for future protocols that demand higher spectral efficiencies to handle the projected user densities and the ever-increasing demand for higher data rates [3], [4]. Specifically, the cyclic prefix reduces the system's spectral efficiency, especially for channels with large delay spread and/or when a small packet size is used [5]. Another aspect that decreases the spectral efficiency is that of excessive out-of-band emissions (OOBE) [6], necessitating the use of guard bands. Other issues such as sensitivity to receiver synchronization errors [7] and high peak to average power ratio (PAPR) [8] further reduce the suitability of CP-OFDM.

Of the many available waveforms, filter bank multi-carrier with offset quadrature amplitude modulation (FBMC-OQAM) is being strongly considered as an alternative to CP-OFDM [9], its main advantage being its increased spectral efficiency (as the cyclic prefix is no longer present) and very low OOBE (due to use of the per sub-carrier filtering). It has also been shown to have a greater immunity to

The associate editor coordinating the review of this manuscript and approving it for publication was Mahdi Zareei.

frequency synchronization errors, making it a very attractive option [6].

FBMC achieves its spectral efficiency improvement by the use of smooth pulse shaping filters (typically based on a prototype filter) on each sub-carrier, resulting in reduced OOBE. However, in this new parallel filter bank arrangement we no longer have a set of orthogonal sub-carriers; rather, they interfere with each other both in frequency and in time. To deal with this, the solution employed in FBMC-OQAM is to stagger, by half a symbol interval, the modulation of real-valued data symbols onto the in-phase and quadrature components of each sub-carrier. Then, by judicious pulse shaping filter design, it is arranged for the interference appearing on the outputs from a bank of matched filters in a receiver to be purely imaginary, thereby preserving orthogonality between the real-valued symbols on each of the quadrature components. Some well-known prototype filter designs include PHYDYAS [10], Hermite [11], root raised cosine (RRC) [12] and half cosine [13].

This purely imaginary interference plays an important role in channel estimation and also contributes to errors in receivers with imperfect channel state information (CSI). Thus an accurate and efficient channel estimation (CE) procedure is an essential part of the successful operation of an FBMC-OQAM system. The most widely established preamble-based CE techniques for FBMC-OQAM follow a virtual symbol (VS) approach often applied to the pilot structures in either the interference approximation method (IAM) [14] or the interference cancellation method (ICM) [15].

However, these schemes suffer from a severe CE mean-squared error (CE-MSE) floor at high SNR (>20 dB) which ultimately limits the performance. This is due to the combined effect of several simplifying assumptions made in the development of the VS method, namely: 1) the assumption of zero interference from the data portion of the burst on the preamble, 2) the assumption of a locally invariant channel in a small frequency-time (FT) neighborhood, and 3) an assumption that the interference and noise contributions present at the output from each matched filter are both uncorrelated [8], [16], [17].

In this paper, we propose a parameterizable CE scheme, called GLS-u, based on generalized least squares (GLS) estimation [20], [21], which generates each channel estimate based on a number of consecutive matched filter outputs while taking fully into account the correlated nature of the noise and interference components present in these matched filter outputs. The proposed technique is compatible with the IAM and ICM pilot structures while resulting in a significantly reduced CE-MSE. We also present a theoretical analysis of the CE-MSE of the proposed GLS method and, for comparison, the conventional VS method. Our analysis differs from previous works such as [16], [17], [22] in that we take into account the correlated nature of the noise and interference across neighboring sub-carriers and the impact of the data interference on all of the CE algorithms considered. Symmetry properties of the intrinsic interference coefficients of the FBMC-OQAM system are proved and used in characterizing the autocorrelation matrices of the interference and noise. The CE-MSE analysis is validated through simulation, and it is also demonstrated through extensive bit error rate (BER) simulations that these CE-MSE gains translate into a significant BER improvement.

The contributions of this paper represent a significant extension of our previous work reported in [18]. The extensions are as follows:

- The GLS-u CE scheme represents a generalization of the CE scheme proposed in [18], where the scheme of [18] corresponds to $u = 2$;
- Symmetry properties of the intrinsic interference coefficient are proved, which can be used to efficiently compute the autocorrelation matrices required by the proposed GLS-based algorithm.
- The simulation study is significantly more comprehensive than that in [18], as it (i) validates the CE-MSE analysis via simulation, (ii) demonstrates the BER gains achievable under various mobility conditions and with different modulation schemes, and (iii) explores the trade-offs afforded by the parameter u.

Notations: Vectors and matrices are denoted by lower and upper case bold letters, respectively. For a matrix $\mathbf{A}$, $[\mathbf{A}]_{i,j}$ denotes its (i, j) entry and for a vector $\mathbf{b}$, b_i denotes its i^{th} entry. Superscripts T and $\mathcal{H}$ denote transpose and conjugate transpose respectively. $\Re(x)$ denotes the real part of a complex number x, while x^* denotes its complex conjugate. $\mathbb{Z}$ denotes the set of integers, $\mathbb{E}$ denotes the expectation operator, and $j = \sqrt{-1}$.

II. FBMC-OQAM SYSTEM MODEL

A. FBMC-OQAM SIGNAL

The discrete-time complex baseband equivalent of an FBMC-OQAM signal [23] having M sub-carriers, at time $t = l\frac{T_s}{M}$ seconds, is given by

$$s(l) = \sum_{m=0}^{M-1} \sum_{n=-\infty}^{+\infty} a_{m,n} g_{m,n}(l) \,, \tag{1}$$

where a real-valued symbol $a_{m,n}$ is modulated onto the m^{th} sub-carrier at time $n \cdot \frac{T_s}{2}$ seconds, i.e., $\frac{1}{T_s}$ is the equivalent rate of complex-valued symbols on each sub-carrier. The m^{th} sub-carrier has centre frequency $m \cdot \frac{1}{2T_s}$ Hertz, and the pair (m, n) indexes the corresponding frequency-time (FT) resource element. Each $g_{m,n}(l)$ is a phase, frequency and time shifted version of a prototype impulse response $g(l)$ which, assuming M is even, can be expressed as

$$g_{m,n}(l) \triangleq g\left(l - \frac{nM}{2}\right) e^{j\frac{2\pi}{M} m(l - \frac{L_g - 1}{2})} e^{j\varphi_{m,n}} \,, \tag{2}$$

where g is a real linear-phase unit-energy waveform with length $L_g = KM + 1$, and $\varphi_{m,n} \triangleq (m + n)\frac{\pi}{2} + mn\pi$. Thus

$$s(l) = \sum_{m=0}^{M-1} \sum_{n=-\infty}^{+\infty} a_{m,n} j^{m+n} e^{j2\pi \frac{ml}{M}} g(l - \frac{nM}{2}) \beta_{m,n} \,, \tag{3}$$

where $\beta_{m,n} \triangleq e^{j2\pi m(\frac{n}{2} - \frac{KM-1}{2M})}$. This is illustrated in Fig.1.

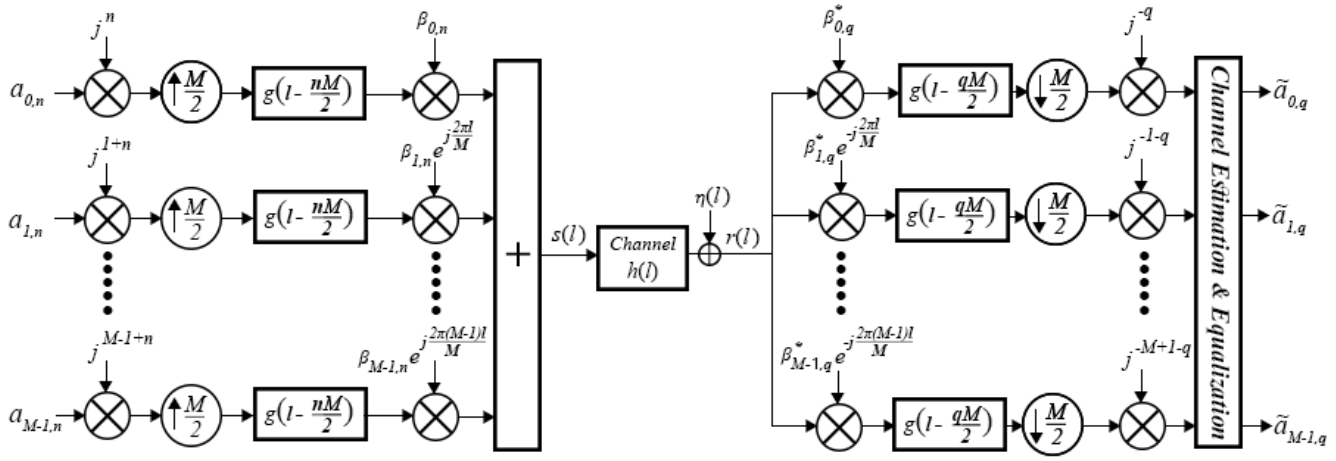

FIGURE 1. FBMC-OQAM system model.

TABLE 1. Tabulated values of $\xi_{m,n}^{p,q}$ for the PHYDYAS filter [10], for p even. The entries marked with † are negated for p odd. We have approximated values with $|\xi_{p,q}^{m,n}| \leq 0.0003$ to zero.

	q-3	q-2	q-1	n=q	q+1	q+2	q+3
p+3	0	0	0	0	0	0	0
p+2	j0.0006†	0	0	0	0	0	-j0.0006†
p+1	-j0.0429†	-j0.125	-j0.2058†	-j0.2393	-j0.2058†	-j0.125	-j0.0429†
m=p	j0.0668†	0	j0.5644†	1	-j0.5644†	0	-j0.0668†
p-1	-j0.0429†	j0.125	-j0.2058†	j0.2393	-j0.2058†	j0.125	-j0.0429†
p-2	j0.0006†	0	0	0	0	0	-j0.0006†
p+4	0	0	0	0	0	0	0

A matched filter receiver attempting to detect symbol $a_{p,q}$ has response $g_{p,q}^*$ and its output will contain contributions from each transmitted symbol $a_{m,n}$ given by $a_{m,n}\xi_{m,n}^{p,q}$, where the intrinsic interference coefficient $\xi_{m,n}^{p,q}$ is defined as

$$\xi_{m,n}^{p,q} \triangleq \sum_{l=-\infty}^{\infty} g_{m,n}(l) g_{p,q}^*(l) \,. \tag{4}$$

As per [23], the prototype filter is assumed to be designed such that the following real orthogonality condition is satisfied:

$$\Re(\xi_{m,n}^{p,q}) = \Re\left(\sum_{l=-\infty}^{\infty} g_{m,n}(l) g_{p,q}^*(l)\right) = \delta_{m,p}\delta_{n,q} \,, \tag{5}$$

where $\delta_{r,s}$ denotes the Kronecker delta function. This condition causes the matched filter output to contain *purely imaginary intrinsic interference*. This is illustrated in Table 1 for the case of the PHYDYAS filter [10]. Tables of $\xi_{m,n}^{p,q}$ for other prototype filters, e.g. Hermite [11], root raised cosine [12] and half cosine [13], can be found in Appendix A.

B. RECEPTION WITH TIME-DISPERSIVE CHANNEL

This paper is concerned with preamble-based channel estimation techniques, and thus the time-dispersive channel is assumed to be time-invariant for the duration of the preamble and the first data-bearing symbols. Additionally, under the mild assumption that the channel delay spread is small compared to the FMBC. symbol duration, we can define a channel vector $\mathbf{h} = [h_0\ h_1\ \cdots\ h_{M-1}]$ where h_i is the channel gain of the i^{th} sub-carrier, and is normalized such that $\mathbb{E}[|h_i|^2] = 1$. The output of the $(p, q)^{th}$ matched filter is

$$\begin{aligned} y_{p,q} &= \sum_{m,n} h_m \xi_{m,n}^{p,q} a_{m,n} + w_{p,q} \\ &= h_p a_{p,q} + \sum_{(m,n)\neq(p,q)} h_m \xi_{m,n}^{p,q} a_{m,n} + w_{p,q} \,, \end{aligned} \tag{6}$$

where the so-called "intrinsic interference" from neighboring symbols is given by

$$i_{p,q} \triangleq \sum_{(m,n)\neq(p,q)} h_m \xi_{m,n}^{p,q} a_{m,n} \,, \tag{7}$$

and $w_{p,q} = \sum_l \eta(l) g_{p,q}^*(l)$ is a filtered version of complex white Gaussian noise $\eta(l) \sim \mathcal{N}(0, \sigma^2)$ and thus represents a colored additive Gaussian noise component affecting the reception of symbol $a_{p,q}$. The covariance of $w_{p,q}$ is $\mathbb{E}[w_{p,q} w_{m,n}^*] = \sigma^2 \xi_{m,n}^{p,q}$.

If $\tilde{\mathbf{h}} \approx \mathbf{h}$ is an estimate of the channel vector, then by ignoring the interference term, a one-tap zero-forcing equalizer can be used to estimate the data symbols via

$$\tilde{a}_{p,q} \triangleq \Re\left(\frac{y_{p,q}}{\tilde{h}_p}\right) \approx a_{p,q}. \tag{8}$$

This paper considers preamble-based approaches which are used to form the channel estimates $\tilde{\mathbf{h}}$ required for the above channel equalizer.

C. SYMMETRY PROPERTIES OF $\xi_{m,n}^{p,q}$

In this paper, we will make use of various symmetry and translation properties of $\xi_{m,n}^{p,q}$, which are given in the following theorem.

Theorem 1: For any $m, n, p, q, \delta_p, \delta_q \in \mathbb{Z}$ we have:

$$\textit{Conjugate Symmetry:} \quad \xi_{m,n}^{p,q} = \left(\xi_{p,q}^{m,n}\right)^* \tag{9}$$

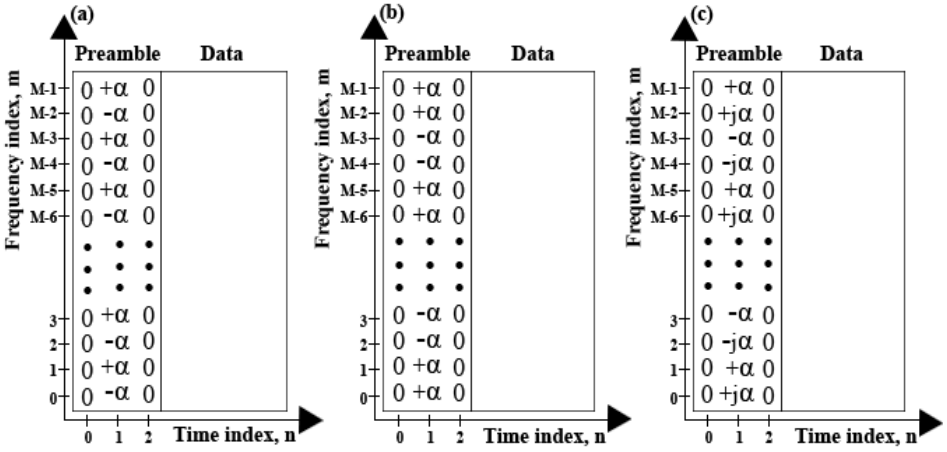

FIGURE 2. Preamble arrangement of (a) ICM; (b) IAM-R; and (c) IAM-C [8]. Here α is a real-valued symbol.

$$\textit{Frequency Symmetry:}\quad \xi^{p,q}_{p-\delta_p,n} = (-1)^{n-q}\left(\xi^{p,q}_{p+\delta_p,n}\right)^* \tag{10}$$

$$\textit{Time Symmetry:}\quad \xi^{p,q}_{m,q-\delta_q} = (-1)^{(1+m-p)\delta_q}\xi^{p,q}_{m,q+\delta_q} \tag{11}$$

$$\textit{Frequency Translation:}\quad \xi^{p+\delta_p,q}_{m+\delta_p,n} = \xi^{p,q}_{m,n} \tag{12}$$

$$\textit{Time Translation:}\quad \xi^{p,q+\delta_q}_{m,n+\delta_q} = (-1)^{(m-p)\delta_q}\xi^{p,q}_{m,n}. \tag{13}$$

A detailed proof of *Theorem 1* is given in Appendix B.

Some previous works (e.g. [14]–[16]) have used the frequency symmetry property in the immediate FT neighbourhood ($\delta_p = \pm 1$), and in [8] some of these symmetries were shown to exist in a 5×3 frequency-time neighborhood. However, the symmetry properties given in Theorem 1 hold for *any* FT grid and for *any* prototype filter.

III. PREAMBLE-BASED CHANNEL ESTIMATION

A. VIRTUAL SYMBOL APPROACH

Fig. 2 shows the preamble symbol arrangements of ICM, IAM-R and IAM-C, where α is a real-valued preamble symbol [8]. For such a preamble structure, a simple method to estimate the channel is to assume that for each sub-carrier p, the sub-carrier gain h_p is constant over the immediate sub-carrier neighborhood, i.e.,

$$\begin{aligned} y_{p,q} &\approx h_p \sum_{(m,n)\in\Theta_{p,q}} \xi^{p,q}_{m,n} a_{m,n} + \sum_{(m,n)\notin\Theta_{p,q}} h_m \xi^{p,q}_{m,n} a_{m,n} + w_{p,q} \\ &\triangleq h_p c_{p,q} + i_{p,q} + w_{p,q}\ , \end{aligned} \tag{14}$$

where $\Theta_{p,q}$ is the set of neighboring FT points around (p, q) where $\xi^{p,q}_{m,n}$ has a significant magnitude, and $i_{p,q}$ is the interference contribution from all symbols outside the $\Theta_{p,q}$ neighbourhood including other pilots and the random symbols in the data portion of the burst. For example, for the PHYDYAS prototype filter and with reference to Table 1, the works of [14], [15] considered $\Theta_{p,q} \triangleq \{(m, n) : |p - m| \le 1, |q - n| \le 1\}$; we note that here $i_{p,q}$ will be dominated by the random symbols in the burst (and not by the other pilots).

TABLE 2. Virtual symbol c_p and corresponding MSE floors for various preamble structures, for the PHYDYAS prototype filter.

Scheme	$c_{p,q} \triangleq \sum_{(m,n)\in\Theta_{p,q}} \xi^{p,q}_{m,n} a_{m,n}$	$\lvert c_p\rvert$	MSE floor (relative to ICM), from (29)
ICM	$c_p{=}a_{p,1}$	$\lvert\alpha\rvert$	0 dB
IAM-R	$c_p{=}a_{p,1}\left(1 \pm 2\xi^{p,1}_{p+1,1}\right)$	$\approx 1.11\lvert\alpha\rvert$	-0.9 dB
IAM-C	$c_p{=}a_{p,1}\left(1 \pm j2\xi^{p,1}_{p+1,1}\right)$	$\approx 1.48\lvert\alpha\rvert$	-3.4 dB

For the three preamble structures in Fig. 2, channel estimation is performed only using pilot symbols at time instant $q = 1$. Thus, for simplicity we define $y_p \triangleq y_{p,1}$, $c_p \triangleq c_{p,1}$, $i_p \triangleq i_{p,1}$ and $w_p \triangleq w_{p,1}$, leading to the channel estimate

$$\tilde{h}_p \triangleq \frac{y_p}{c_p} \approx \frac{h_p c_p + i_p + w_p}{c_p} \approx h_p\ , \tag{15}$$

where the second approximation is due to the usual practice in the virtual symbol approach of ignoring the impact of i_p [14], [15]. Using (10) and the relevant $\xi^{p,q}_{m,n}$ table (e.g., Table 1 for the PHYDYAS filter, or Tables 4, 5 or 6 for other filters), formulae for c_p for each of the three schemes (ICM, IAM-R and IAM-C) can be computed. The result is illustrated in Table 2 for the specific case of the PHYDYAS filter [10].

B. GENERALIZED LEAST SQUARES BASED CHANNEL ESTIMATION

This subsection describes the proposed algorithm, called GLS-u, which estimates h_p based on the outputs from u consecutive matched filters indexed from $p - L_1$ to $p + L_2$, i.e., $u = 1 + L_1 + L_2$. For u odd we take $L_1 = L_2$, while for u even we assume $L_1 = L_2 - 1$.

Defining the vector $\mathbf{y}_p = \left[y_{p-L_1} \ldots y_p \ldots y_{p+L_2}\right]^T$ and under the assumption that the channel is locally constant over the u sub-carriers (and their Θ regions), we have

$$\mathbf{y}_p \approx \mathbf{c}_p h_p + \mathbf{i}_p + \mathbf{w}_p\ , \tag{16}$$

where $\mathbf{c}_p = \left[c_{p-L_1} \dots c_p \dots c_{p+L_2}\right]^T$ is a vector of virtual symbols as defined in Section III-A with $\mathbf{i}_p$ and $\mathbf{w}_p$ being similarly defined. Note that $\mathbf{i}_p$ contains contributions from both pilots and data symbols; however, for well-designed prototype filters the interference from the other pilot symbols is negligible and thus we can safely only consider contributions from the random data symbols $a_{m,n}$ – these are independent zero-mean random variables with variance σ_a^2.

From (16) we see that $\mathbf{y}_p$ contains weighted observations of the unknown h_p perturbed by additive correlated random terms $\mathbf{i}_p + \mathbf{w}_p$; as such, the generalized least squares (GLS) approach may be applied. In this context, GLS has a clear advantage over ordinary least squares (OLS) due to the correlated nature of the perturbations.

Denote by $\mathbf{\Omega}_p$ the autocorrelation matrix of $\mathbf{i}_p + \mathbf{w}_p$; the GLS estimate of h_p is given by

$$\bar{h}_p = \left(\mathbf{c}_p^{\mathcal{H}} \mathbf{\Omega}_p^{-1} \mathbf{c}_p\right)^{-1} \mathbf{c}_p^{\mathcal{H}} \mathbf{\Omega}_p^{-1} \mathbf{y}_p \,. \tag{17}$$

There is a difficulty in implementing the above estimator, as knowledge of the channel is required in order to compute the matrix $\mathbf{\Omega}_p$. We therefore define $\mathbf{\Omega}$, an approximation to $\mathbf{\Omega}_p$, in Section III-C, leading to the following GLS-based channel estimator:

$$\tilde{h}_p = \mathbf{g}_p^T \mathbf{y}_p \triangleq \left(\mathbf{c}_p^{\mathcal{H}} \mathbf{\Omega}^{-1} \mathbf{c}_p\right)^{-1} \mathbf{c}_p^{\mathcal{H}} \mathbf{\Omega}^{-1} \mathbf{y}_p \,. \tag{18}$$

As $\mathbf{g}_p$ can be computed *a priori*, and $\tilde{h}_p$ is simply a linear combination of the u elements of $\mathbf{y}_p$, (18) can be implemented with low complexity. In particular, in comparison to the VS based approach, GLS-u will require an additional $u-1$ multiplications to obtain each channel estimate.

C. AUTOCORRELATION MATRIX FOR $\mathbf{w}_p + \mathbf{i}_p$

To compute the approximation $\mathbf{\Omega}$ of the autocorrelation matrix of the noise plus interference, we proceed by considering the autocorrelation matrix of the noise and interference components separately.

1) AUTOCORRELATION MATRIX FOR $\mathbf{w}_p$

In FBMC-OQAM, the filtered noise is correlated among sub-carriers. The filtered noise at FT point $(p,1)$ is $w_p = \sum_l \eta(l) g_{p,1}^*(l)$, which can be written as

$$w_p = \sum_l \eta(l) g(l - \frac{M}{2}) e^{-j\frac{2\pi}{M}p(l-\frac{L_g-1}{2})} e^{-j\varphi_{p,1}} \,. \tag{19}$$

We have $\mathbb{E}[w_p] = 0$. Also, using (4), the covariance $\mathrm{Cov}[w_{p_1}, w_{p_2}] = \mathbb{E}[w_{p_1} w_{p_2}^*]$, can be computed as

$$\mathrm{Cov}[w_{p_1}, w_{p_2}] = \sigma^2 \sum_l g_{p_1,1}^* g_{p_2,1} = \sigma^2 \xi_{p_1,1}^{p_2,1} \,. \tag{20}$$

The $u \times u$ autocorrelation matrix $\mathbf{B}^{(p)} \triangleq \mathbb{E}\{\mathbf{w}_p \mathbf{w}_p^H\}$, where $\mathbf{w}_p \triangleq [w_{p-L_1} \;\cdots\; w_p \;\cdots\; w_{p+L_2}]^T$ is the vector of noise terms centered at p as per Section III-B, is given by $\mathbf{B}^{(p)} =$

$$\sigma^2 \begin{bmatrix} 1 & \xi_{p-L_1,1}^{p-L_1+1,1} & \xi_{p-L_1,1}^{p-L_1+2,1} & \cdots & \xi_{p-L_1,1}^{p+L_2,1} \\ \xi_{p-L_1+1,1}^{p-L_1,1} & 1 & \xi_{p-L_1+1,1}^{p-L_1+2,1} & \cdots & \xi_{p-L_1+1,1}^{p+L_2,1} \\ \xi_{p-L_1+2,1}^{p-L_1,1} & \xi_{p-L_1+2,1}^{p-L_1+1,1} & 1 & \cdots & \xi_{p-L_1+2,1}^{p+L_2,1} \\ \vdots & \vdots & \vdots & \ddots & \vdots \\ \xi_{p+L_2,1}^{p-L_1,1} & \xi_{p+L_2,1}^{p-L_1+1,1} & \xi_{p+L_2,1}^{p-L_1+2,1} & \cdots & 1 \end{bmatrix} \tag{21}$$

From the frequency translation property (12), it can be shown that the each diagonal is constant, and therefore $\mathbf{B}^{(p)}$ is Toeplitz. Note that (9) implies that $\mathbf{B}^{(p)}$ has conjugate symmetry, and (5) implies that the off-diagonal terms are all purely imaginary, i.e. $\Re(\mathbf{B}^{(p)}) = \mathbf{I}$. Importantly, from (12) it can be shown that $\mathbf{B}^{(p)} = \mathbf{B}^{(p+\delta p)}$, i.e., the autocorrelation matrix is invariant in p; thus we will omit the superscript and define $\mathbf{B} \triangleq \mathbf{B}^{(p)}$.

2) AUTOCORRELATION MATRIX FOR $\mathbf{i}_p$

From (14), the (i,j) element of the $u \times u$ autocorrelation matrix, $\mathbf{C}^{(p)} \triangleq \mathbb{E}\{\mathbf{i}_p \mathbf{i}_p^H\}$, where $\mathbf{i}_p \triangleq [i_{p-L_1} \;\cdots\; i_p \;\cdots\; i_{p+L_2}]^T$ is the vector of interference centred at p as per Section III-B, is given by

$$\begin{aligned}[\mathbf{C}^{(p)}]_{i,j} &= \mathbb{E}[i_{p-L_1+i-1} i_{p-L_1+j-1}^*] \\ &= \sigma_a^2 \sum_{\substack{(m,n)\notin\Theta_{i+\delta,1} \\ (m,n)\notin\Theta_{j+\delta,1}}} \mathbb{E}[|h_m|^2] \xi_{m,n}^{i+\delta,1} (\xi_{m,n}^{j+\delta,1})^* \,,\end{aligned} \tag{22}$$

where σ_a^2 is the variance of the independent data symbols $a_{m,n}$, and $\delta \triangleq p - L_1 - 1$ is used to conveniently index into the vector $\mathbf{i}_p$.

Noting the earlier assumption that $\mathbb{E}[|h_m|^2] = 1$ for every m yields

$$[\mathbf{C}^{(p)}]_{i,j} = \eta\, \sigma^2 \sum_{\substack{(m,n)\notin\Theta_{i+\delta,1} \\ (m,n)\notin\Theta_{j+\delta,1}}} \xi_{m,n}^{i+\delta,1} (\xi_{m,n}^{j+\delta,1})^* \,, \tag{23}$$

where $\eta \triangleq \frac{\sigma_a^2}{\sigma^2}$ is a measure of the receiver's instantaneous signal-to-noise ratio. Note that using property (12) it can be observed the summation in (23) is invariant in p; thus we will omit the superscript and define $\mathbf{C} \triangleq \mathbf{C}^{(p)}$.

3) AUTOCORRELATION MATRIX FOR $\mathbf{w}_p + \mathbf{i}_p$

Combining the results of the previous subsections and noting that $\mathbf{w}_p$ and $\mathbf{i}_p$ are uncorrelated, we obtain[1]

$$\Omega = \mathbf{B} + \mathbf{C} \approx \Omega_p \,. \tag{24}$$

Thus, equations (18), (21), (23) and (24) together define the proposed GLS-u channel estimator.

[1]If the channel autocorrelation matrix is available, then we can obtain $\Omega_p = \mathbf{B} + \mathbf{C}^{(p)}$, using (21) and (22), which would be an exact form of (17).

As an illustrative example, for the GLS-2 estimator and the PHYDYAS prototype filter, the matrix $\mathbf{\Omega}$ is given by

$$\begin{aligned}[\mathbf{\Omega}]_{1,1} &= \sigma_a^2\{|\xi_{p,4}^{p,1}|^2 + 2|\xi_{p+1,3}^{p,1}|^2 + 2|\xi_{p+1,4}^{p,1}|^2 + \eta^{-1}\}\\ [\mathbf{\Omega}]_{1,2} &= \sigma_a^2\{\xi_{p,4}^{p,1}\xi_{p,4}^{*p+1,1} + \xi_{p+1,4}^{p,1}\xi_{p+1,4}^{*p+1,1} + \xi_{p+1,1}^{p,1}\eta^{-1}\}\\ [\mathbf{\Omega}]_{2,2} &= [\mathbf{\Omega}]_{1,1} \text{ and } [\mathbf{\Omega}]_{2,1} = [\mathbf{\Omega}]_{1,2}^* \ . \end{aligned} \tag{25}$$

IV. MSE ANALYSIS OF CE TECHNIQUES

The VS method and the proposed GLS-based method have in common two principal assumptions: a) the channel is locally constant[2]; and b) symbols other than the immediate neighbors contribute negligible interference. The second of these assumptions is weak and leads to a floor in the channel estimation MSE. In this section, we theoretically analyze the normalized MSE in order to enable performance comparison; this is defined as

$$\text{MSE} \triangleq \mathbb{E}\left[\left|\frac{\tilde{h}_p - h_p}{h_p}\right|^2\right]. \tag{26}$$

Note that for an unbiased estimator $\text{MSE} = \text{Var}\left[\frac{\tilde{h}_p}{h_p}\right]$.

4) VIRTUAL SYMBOL METHOD

From (14) and (15), for ICM and IAM-R/C we have

$$y_p = h_p c_p + h_p \sum_{(m,n)\notin\Theta_{p,1}} \xi_{m,n}^{p,1} a_{m,n} + w_{p,1} \tag{27}$$

and so

$$\frac{\tilde{h}_p - h_p}{h_p} = \frac{y_p}{h_p c_p} - 1 = \frac{1}{c_p}\left\{\sum_{(m,n)\notin\Theta_{p,1}} \xi_{m,n}^{p,1} a_{m,n} + w_{p,1}\right\}. \tag{28}$$

The real-valued data symbols $a_{m,n}$ for $n \geq 3$ are uncorrelated zero-mean random variables with variance σ_a^2. Taking the expectation with respect to these data symbols we find that $\mathbb{E}\left[\frac{\tilde{h}_p - h_p}{h_p}\right] = 0$, implying that the estimator is unbiased. The normalized variance (or MSE) is given by

$$\text{MSE}_{\text{VS}} = \frac{\sigma_a^2}{|c_p|^2}\left\{\sum_{(m,n)\notin\Theta_{p,1}} |\xi_{m,n}^{p,1}|^2 + \frac{\sigma^2}{\sigma_a^2}\right\}. \tag{29}$$

From this expression, we see that in the limit as $\sigma^2 \to 0$ (i.e., in high-SNR conditions), there remains an estimator MSE floor that is inversely proportional to the squared magnitude of the virtual symbol c_p. Note that, as per Table 2 (which is computed based on the PHYDYAS filter), this squared magnitude is largest for the IAM-C method, which is why IAM-C has the lowest MSE floor when using the virtual symbol method.

[2]In highly frequency selective channels, the "locally constant channel" assumption also becomes a limiting factor.

5) GLS-BASED ESTIMATION METHOD

Noting that any GLS estimator is unbiased, using (18) we may write the MSE of the proposed GLS-based estimator as

$$\begin{aligned}\text{MSE}_{\text{GLS}} &= \text{Var}\left[\frac{\tilde{h}_p}{h_p}\right] = \mathbf{g}_p^{\mathcal{H}}\mathbb{E}\left[\frac{\mathbf{y}_p}{h_p}\left(\frac{\mathbf{y}_p}{h_p}\right)^{\mathcal{H}}\right]\mathbf{g}_p\\ &\triangleq \mathbf{g}_p^{\mathcal{H}}\hat{\mathbf{\Omega}}\mathbf{g}_p \ . \end{aligned} \tag{30}$$

Substituting the expression for $\mathbf{g}_p$ from (18), and grouping the scalar terms, we obtain

$$\text{MSE}_{\text{GLS}} = \frac{1}{\left|\mathbf{c}_p^{\mathcal{H}}\mathbf{\Omega}^{-1}\mathbf{c}_p\right|^2}\mathbf{c}_p^{\mathcal{H}}\mathbf{\Omega}^{-1}\hat{\mathbf{\Omega}}\left(\mathbf{c}_p^{\mathcal{H}}\mathbf{\Omega}^{-1}\right)^{\mathcal{H}}.$$

From the definition of $\mathbf{y}_p$, it can be shown that $\hat{\mathbf{\Omega}} = \mathbf{\Omega}$; thus

$$\text{MSE}_{\text{GLS}} = \left(\mathbf{c}_p^{\mathcal{H}}\mathbf{\Omega}^{-1}\mathbf{c}_p\right)^{-1}. \tag{31}$$

We note that in high-SNR conditions the matrix $\mathbf{B} \approx \mathbf{0}$ and consequently $\mathbf{\Omega} \approx \mathbf{C}$ which is a independent of the noise variance σ^2. Thus our GLS scheme exhibits an MSE error floor given by $\left(\mathbf{c}_p^{\mathcal{H}}\mathbf{C}^{-1}\mathbf{c}_p\right)^{-1}$. Table 3 provides a comparison of the CE-MSE floor for the various GLS-based CE schemes and for the VS benchmarks, where a baseline of ICM-VS is taken. It can be observed that for each preamble structure, this error floor is much reduced when GLS-u is used, and this reduction is more pronounced as the parameter u is increased.

TABLE 3. CE-MSE floor relative to ICM-VS using PHYDYAS prototype filter.

Scheme	MSE floor, relative to ICM-VS, from (29) and (31)			
	VS	GLS-2	GLS-3	GLS-5
ICM	0 dB	-2.4 dB	-4.1 dB	-8.1 dB
IAM-R	-0.9 dB	-3.9 dB	-5.0 dB	-6.5 dB
IAM-C	-3.4 dB	-6.4 dB	-7.9 dB	-9.4 dB

V. SIMULATION RESULTS AND DISCUSSION

In this section, a simulation study is conducted in MATLAB to compare the performance of different preamble-based channel estimation techniques in terms of CE-MSE and BER, for a low (ITU Indoor A) and a medium (ITU Vehicular A) frequency selective channel model [24], under various mobility conditions.

The transmitted signal consists of $M = 1024$ sub-carriers each having 15kHz bandwidth. The PHYDYAS prototype filter [10] with an overlapping factor of $K = 4$ is considered. Each FBMC frame consists of 3 preamble pilot symbols followed by 32 data symbols as per the structures illustrated in Fig. 2, and we set $\alpha = 1$. For each FBMC-OQAM frame an independent random channel is generated, which varies over the data frame according to the mobility conditions (the channel will be fixed for the frame if there is no mobility). The data modulated on each sub-carrier is generated randomly from either a 4QAM or 16QAM constellation employing Gray coding and normalized such that $\sigma_a^2 = 1$. For each SNR point, 5000 frames are transmitted. Data symbols are

estimated using the estimated channel coefficients and the 1-tap equalizer in (8).

A. CE-MSE RESULTS

Figures 3 and 4 show the CE-MSE for low (ITU Indoor A) and medium (ITU Vehicular A) frequency selective channels, respectively. Simulation results (discrete points labeled "Sim") are shown as well as the evaluated analytical expressions (29) and (31) (continuous curves labeled "Th"). For brevity, the main focus is on the IAM-C structure, as it outperforms the others due to its higher value of $|c_p|$ as previously noted in Table 2.

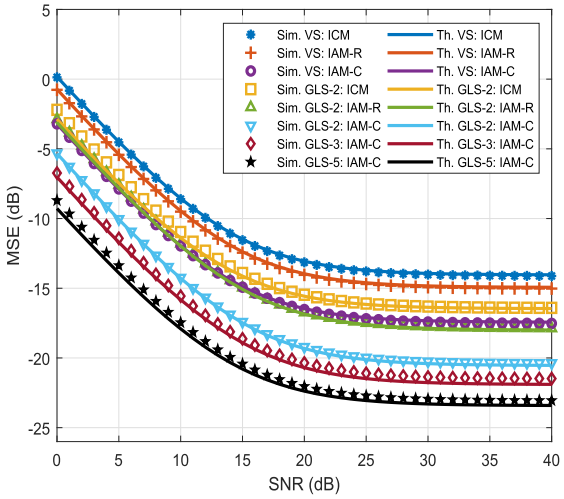

FIGURE 3. Comparison of theoretical and simulated CE-MSE performance among VS and GLS-based channel estimation methods. ICM, IAM-R and IAM-C preamble structures are considered. The channel model is ITU Indoor A.

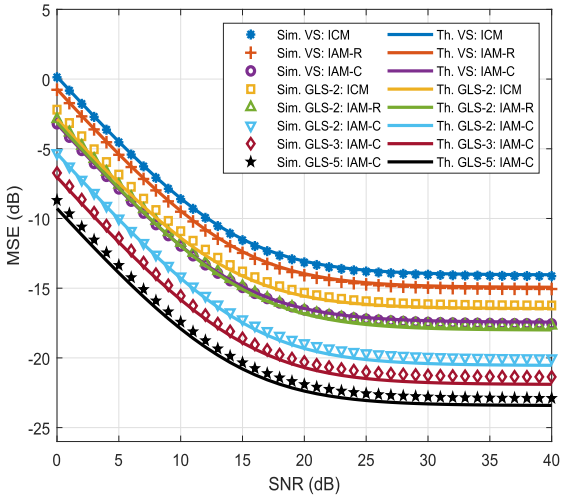

FIGURE 4. Comparison of theoretical and simulated CE-MSE performance among VS and GLS-based channel estimation methods. ICM, IAM-R and IAM-C preamble structures are considered. The channel model is ITU Vehicular A.

From Figures 3 and 4 it can be seen that the proposed GLS-u estimator outperforms the VS estimator for all pilot structures (ICM, IAM-R/C) for low and medium frequency selective channels, with GLS-2 showing almost 3 dB improvement in CE-MSE, and there is near-perfect agreement between the simulation results and (31). The GLS-3 and GLS-5 schemes improve the CE-MSE further, obtaining gains of 4 dB and 5.5 dB respectively compared to the VS estimator. However we note that the agreement between the simulations and (31) is not tight due to the constant channel assumption used in the derivation of (31); this effect becomes more pronounced with increasing u.

As the derivations of (29) and (31) do not consider the impact of frequency selectivity, the corresponding theoretical curves are the same in both CE-MSE figures. However, comparing the simulation results in Figures 3 and 4, we can observe that for the case of moderate frequency selectivity, the constant channel assumption is less accurate and the simulation-based curves exhibit a minor deviation from the theoretical curves; nonetheless, the gains obtained by the GLS-u schemes are still significant.

B. BER RESULTS

As the data symbols are temporally displaced from the pilots, it is necessary to consider the impact of channel coherence time when evaluating BER. Consequently, results are presented here for both low and medium frequency selective channels, each with different mobility conditions, as shown in Figures 5-8. For brevity we focus on the IAM-C pilot arrangement and include results for 4QAM and 16QAM.

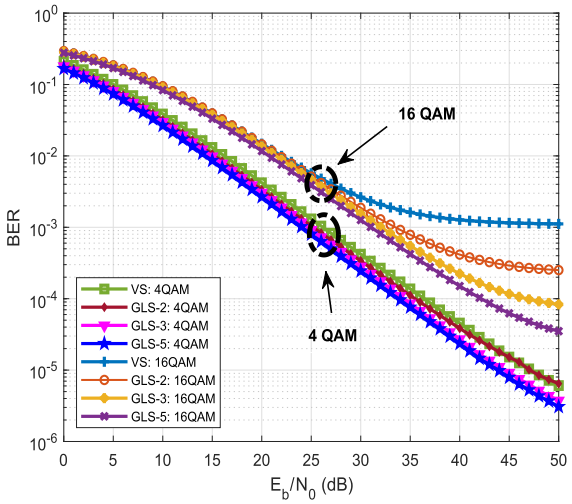

FIGURE 5. BER comparison of systems using GLS and VS channel estimation schemes. Results are shown for 4QAM, and 16QAM modulations. The IAM-C preamble structure is assumed. The channel model is ITU Indoor A, with no mobility.

The BER results for the low frequency selective channel scenario are presented in Figures 5 and 6. It may be observed that the GLS-based CE schemes exhibit BER gains when compared to the corresponding VS scheme. Similar effects can be seen in the BER results for the moderate frequency selectivity scenario, as shown in Figure 7, where again the GLS schemes outperform the VS scheme for 16QAM.

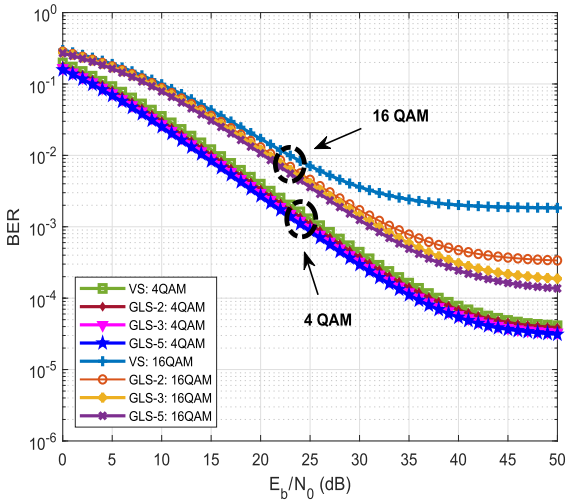

FIGURE 6. BER comparison of systems using GLS and VS channel estimation schemes. Results are shown for 4QAM, and 16QAM modulations. The IAM-C preamble structure is assumed. The channel model is ITU Indoor A, with a mobility of 15km/h.

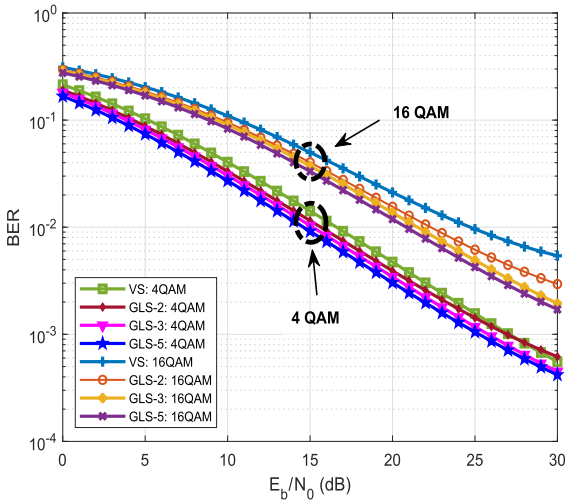

FIGURE 7. BER comparison of systems using GLS and VS channel estimation schemes. Results are shown for 4QAM, and 16QAM. The IAM-C preamble structure is assumed. The channel model is ITU Vehicular A, with no mobility.

With 4QAM modulation, despite the reduced CE-MSE, the GLS-based methods only moderately outperform the VS method under most conditions. Figure 8 shows the effect of mobility on the BER of the GLS-u CE scheme, for $u \in \{2, 3, 5\}$. The effect of mobility on the BER of the VS CE scheme is also shown for comparison. Here the IAM-C preamble structure is assumed, and the channel is ITU Indoor A. At an SNR of 60 dB and with 16QAM modulation, the GLS-based CE schemes exhibit an improvement in BER over the VS approach over the entire range of mobilities considered, with a clear BER advantage achievable from increasing the parameter u in the low-mobility regime.

From Figures 5-7 it can be observed that the BER gain becomes more pronounced as the modulation order increases, which is true even when mobility is present. The reason for

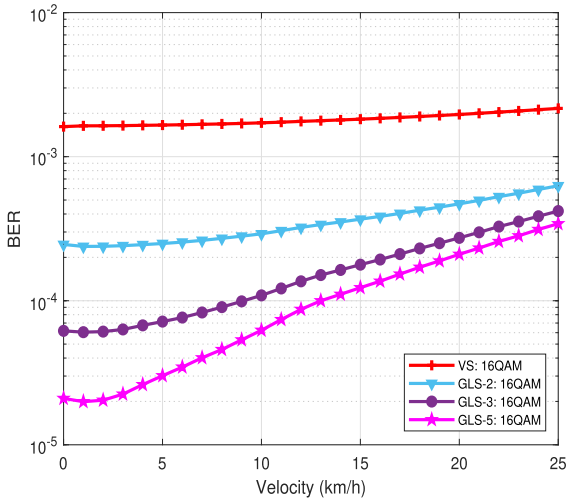

FIGURE 8. BER comparison of systems using GLS, and VS channel estimation schemes. Results are shown for 16QAM modulation. The IAM-C preamble structure is assumed. The channel model is ITU Indoor A at $E_b/N_0 = 60$ dB, with mobility in the range of 0 to 25km/h.

this is that the CE-MSE measure, as defined in (26), captures both amplitude and phase errors in the channel estimate, whereas the performance of constant-amplitude modulation schemes such as 4QAM is not affected by errors in the amplitude of the channel estimate. Thus the CE-MSE measure can only be expected to be a good predictor of BER performance when multi-level constellations such as 16QAM or higher order QAM are used, which is verified by the presented results. From this we may conclude that GLS-based CE scheme is a very attractive option if multi-level signaling is used, making it suitable for high-data-rate FBMC-OQAM applications.

VI. CONCLUSION

In this paper, a novel parameterizable generalized least squares (GLS) based channel estimation scheme was presented, which is capable of taking into account the correlation of noise and interference among sub-carriers. A theoretical analysis of the CE-MSE of this estimator revealed that it exhibits a CE-MSE improvement of up to 6 dB with respect to the virtual symbol based approach. Simulation results demonstrate that for higher-order modulation schemes, this lowering of the CE-MSE results in a significant improvement in the system's bit error rate (BER) performance, making the proposed GLS-based estimator a very attractive option for high-data-rate FMBC-OQAM applications.

APPENDIX A
INTRINSIC INTERFERENCE COEFFICIENT RESPONSE TABLES

This Appendix details the interference coefficients $\xi_{m,n}^{p,q}$ in tabular form for various popular prototype filters mentioned in Section I. Tables 4, 5 and 6 are for Hermite, root raised cosine, and half cosine prototype filters, respectively.

TABLE 4. $\xi_{m,n}^{p,q}$ table for even p using Hermite filter [$K = 4$]. The entries in columns marked with † are negated for p odd.

	q-3†	q-2	q-1†	n=q	q+1†	q+2	q+3†
p+3	0	0	-j0.0054	j0.0098	-j0.0054	0	0
p+2	0	0	j0.0369	0	-j0.0369	0	0
p+1	-j0.0054	j0.037	-j0.2393	-j0.4357	-j0.2393	j0.037	-j0.0054
m=p	j0.0098	0	j0.4357	1	-j0.4357	0	-j0.0098
p-1	-j0.0054	-j0.037	-j0.2393	j0.4357	-j0.2393	-j0.037	-j0.0054
p-2	0	0	j0.0369	0	-j0.0369	0	0
p+4	0	0	-j0.0054	-j0.0098	-j0.0054†	0	0

TABLE 5. $\xi_{m,n}^{p,q}$ table for even p using RRC filter [rolloff $\beta = 0.50$]. The entries in columns marked with † are negated for p odd.

	q-3†	q-2	q-1†	n=q	q+1†	q+2†	q+3
p+3	-j0.0027	0	0	0	0	0	-j0.0027
p+2	j0.0020	0	j0.0004	0	-j0.0004	0	-j0.0020
p+1	-j0.0920	-j0.123	-j0.1503	-j0.1591	-j0.1503	-j0.123	-j0.0920
m=p	j0.1290	0	j0.6021	1	-j0.6021	0	-j0.1290
p-1	-j0.0920	j0.123	-j0.1503	j0.1591	-j0.1503	j0.123	-j0.0920
p-2	j0.0020	0	j0.0004	0	-j0.0004	0	-j0.0020
p+4	-j0.0027	0	0	0	0	0	-j0.0027

TABLE 6. $\xi_{m,n}^{p,q}$ table for even p using half cosine filter. The entries in columns marked with † are negated for p odd.

	q-3†	q-2	q-1†	n=q	q+1†	q+2	q+3†
p+3	-j0.0009	0	0	0	0	0	-j0.0009
p+2	j0.0013	0	0	0	0	0	-j0.0013
p+1	-j0.0006	-j0.1063	-j0.250	-j0.3184	-j0.250	-j0.1063	-j0.0006
m=p	j0.0024	0	j0.500	1	-j0.500	0	-j0.0024
p-1	-j0.0006	j0.1063	-j0.250	j0.3184	-j0.250	j0.1063	-j0.0006
p-2	j0.0013	0	0	0	0	0	-j0.0013
p+4	-j0.0009	0	0	0	0	0	-j0.0009

For ease of presentation, values $|\xi_{p,q}^{m,n}| \leq 0.0003$ have been approximated to zero.

APPENDIX B
PROOF OF THEOREM 1

Preliminaries: Rearranging (2) we obtain

$$g_{m,n}(l) = e^{j(\varphi_{m,n} - m\frac{L_g-1}{M}\pi)} g\left(l - n\frac{M}{2}\right) e^{jm\frac{2\pi}{M}l}.$$

This allows the reformulation of (4) as

$$\xi_{m,n}^{p,q} = e^{j\phi(m,n,p,q)} \sum_{l=-\infty}^{\infty} g\left(l - n\frac{M}{2}\right) g\left(l - q\frac{M}{2}\right) e^{j(m-p)\frac{2\pi}{M}l} \tag{32}$$

where $\phi(m, n, p, q) \triangleq \varphi_{m,n} - \varphi_{p,q} + (p-m)\frac{L_g-1}{M}\pi$.

Proof of (9): This follows immediately from (4).

Proof of (10): From (32) we have

$$\begin{aligned}\xi_{p-\delta_p,n}^{p,q} &= e^{j\phi(p-\delta_p,n,p,q)} \sum_{l=-\infty}^{\infty} g\left(l - n\frac{M}{2}\right) g\left(l - q\frac{M}{2}\right) e^{-j\delta_p\frac{2\pi}{M}l} \\ &= e^{j\phi(p-\delta_p,n,p,q)} \left(e^{-j\phi(p+\delta_p,n,p,q)} \xi_{p+\delta_p,n}^{p,q}\right)^* \\ &= (-1)^{n-q} \left(\xi_{p+\delta_p,n}^{p,q}\right)^*,\end{aligned}$$

as required.

Proof of (11): From (32) we have

$$\begin{aligned}\xi_{m,q-\delta_q}^{p,q} &= e^{j\phi(m,q-\delta_q,p,q)} \sum_{l=-\infty}^{\infty} g\left(l - (q-\delta_q)\frac{M}{2}\right) \\ &\quad \times g\left(l - q\frac{M}{2}\right) e^{j(m-p)\frac{2\pi}{M}l} \\ &= e^{j\phi(m,q-\delta_q,p,q)} e^{j(m-p)q\pi} \sum_{u=-\infty}^{\infty} g\left(u + \delta_q\frac{M}{2}\right) \\ &\quad \times g(u)\, e^{j(m-p)\frac{2\pi}{M}u}.\end{aligned}$$

Similarly we have

$$\begin{aligned}\xi_{m,q+\delta_q}^{p,q} &= e^{j\phi(m,q+\delta_q,p,q)} \sum_{l=-\infty}^{\infty} g\left(l - (q+\delta_q)\frac{M}{2}\right) \\ &\quad \times g\left(l - q\frac{M}{2}\right) e^{j(m-p)\frac{2\pi}{M}l} \\ &= e^{j\phi(m,q+\delta_q,p,q)} e^{j(m-p)(q+\delta_q)\pi} \\ &\quad \times \sum_{u=-\infty}^{\infty} g(u)\, g\left(u + \delta_q\frac{M}{2}\right) e^{j(m-p)\frac{2\pi}{M}u}.\end{aligned}$$

The summations in the two previous results are the same, thus

$$\begin{aligned}\xi_{m,q-\delta_q}^{p,q} &= e^{j\phi(m,q-\delta_q,p,q)} e^{j(m-p)q\pi} e^{-j\phi(m,q+\delta_q,p,q)} \\ &\quad \times e^{-j(m-p)(q+\delta_q)\pi} \xi_{m,q+\delta_q}^{p,q} \\ &= e^{-j\delta_q\pi} e^{-j(m-p)\delta_q\pi} \xi_{m,q+\delta_q}^{p,q} \\ &= (-1)^{(1+m-p)\delta_q} \xi_{m,q+\delta_q}^{p,q},\end{aligned}$$

as required.

Proof of (12): Using (32) we have

$$\begin{aligned}\xi_{m+\delta_p,n}^{p+\delta_p,q} &= e^{j\phi(m+\delta_p,n,p+\delta_p,q)} \\ &\quad \times \sum_{l=-\infty}^{\infty} g\left(l - n\frac{M}{2}\right) g\left(l - q\frac{M}{2}\right) \\ &\quad \times e^{j((m+\delta_p)-(p+\delta_p))\frac{2\pi}{M}l},\end{aligned}$$

since $\phi(m+\delta_p, n, p+\delta_p, q) = \phi(m, n, p, q)$. Thus

$$\begin{aligned}\xi_{m+\delta_p,n}^{p+\delta_p,q} &= e^{j\phi(m,n,p,q)} \sum_{l=-\infty}^{\infty} g\left(l - n\frac{M}{2}\right) g\left(l - q\frac{M}{2}\right) e^{j(m-p)\frac{2\pi}{M}l} \\ &= \xi_{m,n}^{p,q},\end{aligned}$$

as required.

Proof of (13): Using (32) we have

$$\begin{aligned}\xi_{m,n+\delta_q}^{p,q+\delta_q} &= e^{j\phi(m,n+\delta_q,p,q+\delta_q)} \sum_{l=-\infty}^{\infty} g\left(l - (n+\delta_q)\frac{M}{2}\right) \\ &\quad \times g\left(l - (q+\delta_q)\frac{M}{2}\right) e^{j(m-p)\frac{2\pi}{M}l}.\end{aligned}$$

Since $\phi(m, n+\delta_q, p, q+\delta_q) = \phi(m, n, p, q)$ and applying the change of variable $(u - q\frac{M}{2}) = (l - (q + \delta_q)\frac{M}{2})$ we obtain

$$\begin{aligned}\xi_{m,n+\delta_q}^{p,q+\delta_q} &= e^{-j(m-p)(\delta_p)\pi} e^{j\phi(m,n,p,q)} \\ &\quad \times \sum_{u=-\infty}^{\infty} g\left(u - q\frac{M}{2}\right) g\left(u - n\frac{M}{2}\right) e^{j(m-p)\frac{2\pi}{M}l} \\ &= (-1)^{(m-p)\delta_q} \xi_{m,n}^{p,q},\end{aligned}$$

as required; this completes the proof.

REFERENCES

[1] P. Schniter, "Low-complexity equalization of OFDM in doubly selective channels," *IEEE Trans. Signal Process.*, vol. 52, no. 4, pp. 1002–1011, Apr. 2004.
[2] T. Hwang, C. Yang, G. Wu, S. Li, and G. Y. Li, "OFDM and its wireless applications: A survey," *IEEE Trans. Veh. Technol.*, vol. 58, no. 4, pp. 1673–1694, May 2009.
[3] Q. C. Li, H. Niu, A. T. Papathanassiou, and G. Wu, "5G network capacity: Key elements and technologies," *IEEE Veh. Technol. Mag.*, vol. 9, no. 1, pp. 71–78, Mar. 2014.
[4] J. G. Andrews, S. Buzzi, W. Choi, S. V. Hanly, A. Lozano, A. C. K. Soong, and J. C. Zhang, "What will 5G be?" *IEEE J. Sel. Areas Commun.*, vol. 32, no. 6, pp. 1065–1082, Jun. 2014.
[5] A. Müller, "OFDM transmission over time-variant multipath channels," in *Proc. Int. Broadcast. Conv. (IBC)*, Amsterdam, The Netherlands, Sep. 1994, pp. 533–538.
[6] B. Farhang-Boroujeny, "OFDM versus filter bank multicarrier," *IEEE Signal Process. Mag.*, vol. 28, no. 3, pp. 92–112, May 2011.
[7] Y. Medjahdi, M. Terre, D. Le Ruyet, D. Roviras, and A. Dziri, "The impact of timing synchronization errors on the performance of OFDM/FBMC systems," in *Proc. IEEE Int. Conf. Commun. (ICC)*, Kyoto, Japan, Jun. 2011, pp. 1–5.
[8] E. Kofidis, D. Katselis, A. Rontogiannis, and S. Theodoridis, "Preamble-based channel estimation in OFDM/OQAM systems: A review," *Signal Process.*, vol. 93, no. 7, pp. 2038–2054, Jul. 2013.
[9] P. Banelli, S. Buzzi, G. Colavolpe, A. Modenini, F. Rusek, and A. Ugolini, "Modulation formats and waveforms for 5G networks: Who will be the heir of OFDM?: An overview of alternative modulation schemes for improved spectral efficiency," *IEEE Signal Process. Mag.*, vol. 31, no. 6, pp. 80–93, Nov. 2014.
[10] M. G. Bellanger, "Specification and design of a prototype filter for filter bank based multicarrier transmission," in *Proc. IEEE Int. Conf. Acoust., Speech, Signal Process.*, Salt Lake City, UT, USA, May 2001, pp. 2417–2420.
[11] R. Haas and J.-C. Belfiore, "A time-frequency well-localized pulse for multiple carrier transmission," *Wireless Pers. Commun.*, vol. 5, no. 1, pp. 1–18, Jan. 1997.
[12] B. Farhang-Boroujeny, *Signal Processing Techniques for Software Radios*. Raleigh, CA, USA: Lulu, 2008.
[13] J. Du and S. Signell, "Classic OFDM systems and pulse-shaping OFDM/OQAM systems," KTH Roy. Inst. Technol., Stockholm, Sweden, Tech. Rep. TRITA-ICT/ECS R 07:01, 2007, pp. 1–32.
[14] D. Lacroix and J. P. Javaudin, "A new channel estimation method for OFDM/OQAM," in *Proc. 7th Int. OFDM Workhop*, Hamburg, Germany, Sep. 2002, pp. 1–5.
[15] S. Kang and K. Chang, "A novel channel estimation scheme for OFDM/OQAM-IOTA system," *Electron. Telecommun. Res. Inst. J.*, vol. 29, no. 4, pp. 430–436, Aug. 2007.
[16] C. Lélé, J.-P. Javaudin, R. Legouable, A. Skrzypczak, and P. Siohan, "Channel estimation methods for preamble-based OFDM/OQAM modulations," *Eur. Trans. Telecommun.*, vol. 19, no. 7, pp. 741–750, Nov. 2008.
[17] D. Katselis, E. Kofidis, A. Rontogiannis, and S. Theodoridis, "Preamble-based channel estimation for CP-OFDM and OFDM/OQAM systems: A comparative study," *IEEE Trans. Signal Process.*, vol. 58, no. 5, pp. 2911–2916, May 2010.
[18] V. K. Singh, M. F. Flanagan, and B. Cardiff, "Generalized least squares based channel estimation for high data rate FBMC-OQAM," in *Proc. 25th Int. Conf. Telecommun. (ICT)*, St. Malo, France, Jun. 2018, pp. 583–587.
[19] Y.-S. Lee, H.-N. Kim, S. I. Park, and S. I. Lee, "Noise reduction for channel estimation based on pilot-block averaging in DVB-T receivers," *IEEE Trans. Consum. Electron.*, vol. 52, no. 1, pp. 51–58, Feb. 2006.
[20] T. Kariya and H. Kurata,*Generalized Least Squares*. Chichester, U.K.: Wiley, 2004.
[21] S. K. Sengijpta, "Fundamentals of statistical signal processing: Estimation theory," *Technometrics*, vol. 37, no. 4, pp. 465–466, 1995.
[22] D. Katselis, C. R. Rojas, M. Bengtsson, and H. Hjalmarsson, "Frequency smoothing gains in preamble-based channel estimation for multicarrier systems," *Signal Process.*, vol. 93, no. 9, pp. 2777–2782, Sep. 2013.
[23] A. Viholainen, M. Bellanger, and M. Huchard, "PHYDYAS project, deliverable 5.1: Prototype filter and structure optimization," Phys. Layer Dyn. Access Cogn. Radio, Paris, France, Tech. Rep. FP7-ICT, 2009.
[24] R. Jain, "Channel models: A tutorial," in *WiMAX Forum AATG*. St. Louis, MO, USA: Washington Univ. St. Louis, Dept. CSE, 2007.

VIBHUTESH KUMAR SINGH (S'14) received the B.Tech. degree in electronics and communication engineering from the Vellore Institute of Technology (VIT Vellore), India, in 2014, and the M.Tech. degree from the Indraprashtha Institute of Information Technology (IIIT-Delhi), India, in 2016. He is currently pursuing the Ph.D. degree in electrical and electronic engineering with University College Dublin, Ireland, in the field of flexible modulation techniques for future telecommunication networks. He is also an experienced software developer for Windows CE and Desktop environment, and also known for his Technology Blogs, Digital iVision Labs and Circuit Uncle, that connects more than 50,000 people over various social platforms.

MARK F. FLANAGAN (M'03–SM'10) received the B.E. and Ph.D. degrees in electronic engineering from University College Dublin, Ireland, in 1998 and 2005, respectively. From 1998 to 1999, he was a Project Engineer with Parthus Technologies Ltd. From 2006 to 2008, he held Postdoctoral Research Fellowship positions with the University of Zurich, Switzerland, University of Bologna, Italy, and The University of Edinburgh, U.K. In 2008, he was appointed an SFI Stokes Lecturer in electronic engineering with University College Dublin, where he is currently an Associate Professor. In 2014, he was a Visiting Senior Scientist with the German Aerospace Center, Institute of Communications and Navigation, under a DLR-DAAD Fellowship. His research interests include information theory, wireless communications, and signal processing. He has served on the technical program committees for several IEEE international conferences. He is also an Executive Editor of the IEEE COMMUNICATIONS LETTERS.

BARRY CARDIFF (M'03–SM'19) received the B.Eng., M.Eng.Sc., and Ph.D. degrees in electronic engineering from University College Dublin, Ireland, in 1992, 1995, and 2011, respectively. He was a Senior Design Engineer and a Systems Architect with Nokia, from 1993 to 2001, moving to Silicon & Software Systems (S3 group) thereafter as a Systems Architect in their Research and Development Division focused on wireless communications and digitally assisted circuit design. Since 2013, he has been an Assistant Professor with University College Dublin. He holds several U.S. patents related to wireless communication. His research interests include in digitally assisted circuit design, and signal processing for wireless and optical communication systems.